ADVANCED FUNCTIONAL MATERIALS
www.afm-journal.de

Comparative Study of Nano-ZSM-5 Catalysts Synthesized in OH^- and F^- Media

*Zhengxing Qin, Louwanda Lakiss, Lubomira Tosheva, Jean-Pierre Gilson, Aurélie Vicente, Christian Fernandez, and Valentin Valtchev**

This study reports the seeded synthesis of MFI-type (ZSM-5) zeolite in fluoride medium at pH = 8.5. Crystal growth kinetics of the resulting zeolite (ZSM-5-F) as a function of seed content and crystallization temperature is studied. The crystallization time is reduced to 1.5 h and crystals with sizes below 200 nm and a Si/Al ratio of 23.6 are obtained. A zeolite with similar characteristics but synthesized in a hydroxyl medium (ZSM-5-OH) is used to evaluate ZSM-5s synthesized in different crystallization media. Their physicochemical properties are compared and particular attention is paid to the nature, number, and distribution of silanol sites. The two zeolites exhibit similar number of Brønsted acid sites; however the material synthesized in a hydroxyl medium contains a substantially larger number of surface and internal silanols that impact significantly its catalytic performance in methanol to hydrocarbon transformation. While the two materials exhibit similar selectivity in methanol transformations, the catalyst synthesized in fluoride medium shows superior activity and resistance to deactivation. The results suggest that seeded synthesis in a fluoride medium can be used for the preparation of superior zeolite catalysts.

1. Introduction

Microporous zeolite-type materials have already been used in industry for half a century.[1] Their catalytic and separation properties are exploited in some of the largest chemical processes, for instance in the oil refining and petrochemicals production.[2] Despite their large industrial application, their properties/synthetic procedures need to be improved to meet growing environmental and technological challenges. While there has been an intense research in the development of post-synthesis modification methods to tailor the properties of premade crystals,[3] the control of zeolite properties during their synthesis remains a desirable and efficient route for their industrial utilization.

The physicochemical properties of zeolites are a function of the chemical composition of the initial gel or solution and the conditions used for their crystallization.[4] In the past several decades, substantial progress has been made in our understanding of the complex zeolite formation mechanism. For example, the synthesis of zeolites can be conducted in both basic (OH^-) and fluoride medium (F^-),[5] but there are fundamental differences in the zeolite formation mechanism for the two media.[6] Unlike conventional zeolite synthesis conducted at high pH, the use of fluoride synthesis approach allows the crystallization of zeolites in slightly acidic to slightly basic medium (pH < 10). The near-neutral pH of the medium leads to two important consequences: (i) minimized number of non-bridging ≡SiO- defects; and (ii) lower supersaturation of the framework-forming species. As a result, the crystals synthesized in fluoride medium possess fewer framework defects.[7] This is advantageous for prolonging the lifetime of zeolite catalysts, since it is known that framework defect sites are prone to retain coke precursors.[8] Bleken *et al.* have recently reported that large ZSM-5 crystals synthesized in fluoride medium showed higher resistance to coke formation compared to ZSM-5 zeolites synthesized in OH^- medium.[9] Another general and remarkable characteristic of the fluoride approach is that the crystals synthesized under fluoride medium are larger because of the lower nucleation rate.[10] While high quality large crystals are very useful for fundamental studies of zeolites, they suffer from significant drawbacks in their commercial applications due to diffusion limitations.[11] Nanozeolites with very few framework defects seem to be excellent candidates to overcome this limitation, but although some success in the preparation of such materials by post-synthesis modification has been achieved,[12] their direct synthesis remain a challenge.

The objective of this study was to prepare nanosized ZSM-5 crystals by direct synthesis in fluoride medium by careful optimization of the synthesis parameters and to evaluate their catalytic performance. Silicalite-1 seeds were added to the precursor gels to reduce crystallization times and to facilitate the synthesis of nanosized crystals.[13] The content of framework defects of samples prepared by OH^- and F^- routes of similar characteristics

Dr. Z. Qin, Dr. L. Lakiss, Prof. J.-P. Gilson, Dr. A. Vicente, Prof. C. Fernandez, Prof. V. Valtchev
Laboratoire Catalyse & Spectrochimie
ENSICAEN – Université de Caen – CNRS
6 boulevard du Maréchal Juin, 14050, Caen, France
E-mail: valtchev@ensicaen.fr
Dr. L. Tosheva
Division of Chemistry and Environmental Science
Manchester Metropolitan University
Chester St., Manchester, M1, 5GD, UK

DOI: 10.1002/adfm.201301541

was compared and related to the performance of the materials in the catalytic conversion of methanol-to-hydrocarbons (MTH), a reaction of considerable industrial importance.[14]

2. Results and Discussion

2.1. Synthesis of Initial Materials

2.1.1. Synthesis in Fluoride Medium: Effect of F^- on ZSM-5 Formation

Initially, experiments were performed to study the effect of fluoride species on ZSM-5 formation. Nanosized silicalite-1 crystals with an average size of 80 nm and narrow particle size distribution were used as seeds in the synthesis. Our preliminary results showed that the system 0.142TPABr : 0.135TPAOH : $0.072Al_2O_3$: $1.0SiO_2$: $0.616NH_4F$: $20H_2O$ comprising 5 wt% silicalite-1 seeds yielded high quality ZSM-5 at 423 K. This system was also employed without the addition of NH_4F and subjected to hydrothermal treatment at 423 K. The pH of the system was adjusted to 8.5 by addition of diluted HCl prior to hydrothermal treatment. This pH corresponded to the pH value of the gel when ammonium fluoride was used in the synthesis. However, the material obtained was still amorphous after one month of treatment. On the other hand, the NH_4F-containing seeded gel with similar composition yielded highly crystalline ZSM-5 within 3.5 h. This is a sound proof of the positive impact of F^- on zeolite formation. In order to verify this, the crystallization of the gel that remained amorphous after hydrothermal treatment for one month was interrupted and the usual amount of NH_4F was added. After another 56 h of treatment at 373 K, crystallization was completed and highly crystalline ZSM-5 was obtained (XRD pattern not shown). The set of experimental data unambiguously confirmed that fluoride anions induce a very rapid growth of the seed crystals at pH of 8.5.

The incorporation of fluorine species into the zeolite framework during synthesis in F^- medium has been well established by both solid-state nuclear magnetic resonance (NMR) and single crystal X-ray diffraction (XRD) studies.[15,16] Both methods found that F^- counter anions were present in the $[4^15^26^2]$ units of the MFI-type structure. XRD analysis has revealed the presence of five coordinated Si atoms in the zeolite framework, located in slightly distorted trigonal bipyramid built of four framework oxygen atoms and a fluoride anion.[16] We subjected a highly crystalline ZSM-5 sample to ^{19}F MAS NMR analysis and the spectrum obtained is shown in **Figure 1**. The spectrum exhibits a signal at -64 ppm along with a weaker one at –120 ppm. The peak at –64 ppm is assigned to F^- in a $[4^15^26^2]$ cage,[16] while the signal at –120 ppm is most probably due to the presence of free fluoride anions.[17,18] The peak at about -116 ppm is typical of F^- ions in aqueous NH_4F solutions. In our case, this peak can be attributed to F^- counter ion of NH_4^+ or TPA^+ in the zeolite channels. Besides these two peaks, a very weak signal, most probably originating from impurities, was detected at –80 ppm.

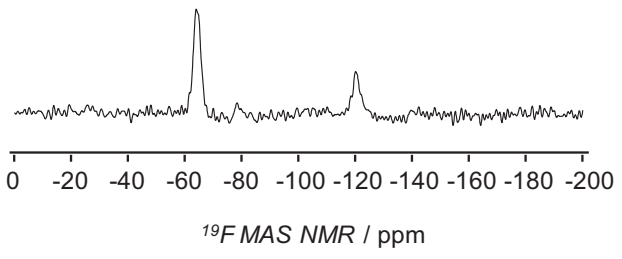

Figure 1. ^{19}F MAS NMR spectrum of highly crystalline ZSM-5 sample synthesized in F^- medium in the presence of 5 wt% seeds.

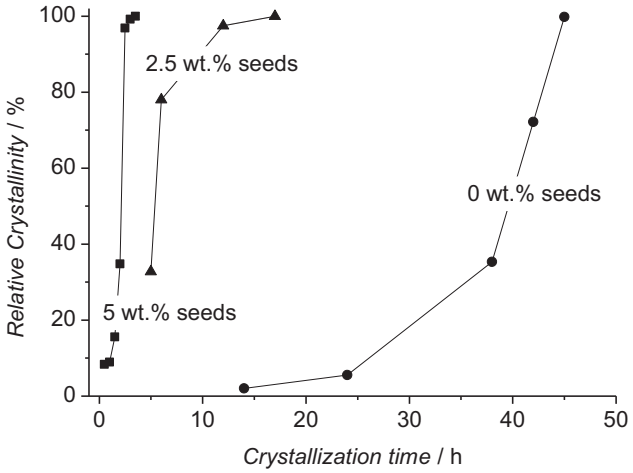

Figure 2. ZSM-5 crystal growth kinetics curves at 423 K from seed-free gels and gels containing 2.5 and 5 wt.% silicalite-1 seeds.

2.1.2. Synthesis in Fluoride Medium: Effect of the Amount of Seeds

A series of experiments were performed at 423 K with gels containing 0, 2.5, and 5 wt% silicalite-1 seeds. **Figure 2** represents the crystal growth curves of these three systems. As can be seen, the crystallization process was strongly dependent on the presence of seeds in the synthesis gels. In the absence of seeds, first traces of crystalline material were detected after ca. 14 h (Figure SI1) and crystallization was completed within 45 h of treatment. The addition of 2.5 wt% silicalite-1 seeds in the initial gel accelerated the crystallization rate. Crystalline material was observed after 5 h of treatment and fully crystalline ZSM-5 was obtained after 17 h (Figure SI2). The crystallization of ZSM-5 zeolite in the presence of 5 wt.% silicalite-1 seeds was much faster. Crystalline MFI-type material was detected after 1 h of treatment and the crystallization was completed within 3.5 h (Figure SI3).

The SEM inspection of the materials prepared with or without seeds showed the presence of uniform crystals in all samples. Their size, however, was different and the largest crystals were observed in the absence of seeds. The crystals were about 3 μm in size with the typical coffin-shape morphology of ZSM-5 (**Figure 3**A). Sub-micrometer crystals were obseved in the sample synthesized with 2.5 wt% seeds. The morphology of the crystals was similar to that of the non-seeded sample, i.e., coffin-shaped crystals with well developed faces (Figure 3B). A further increase of the seed content (5 wt%) resulted in much smaller, ca. 200 nm ZSM-5 crystals (Figure 3C). Again, well shaped crystals were formed, but in this case they were almost

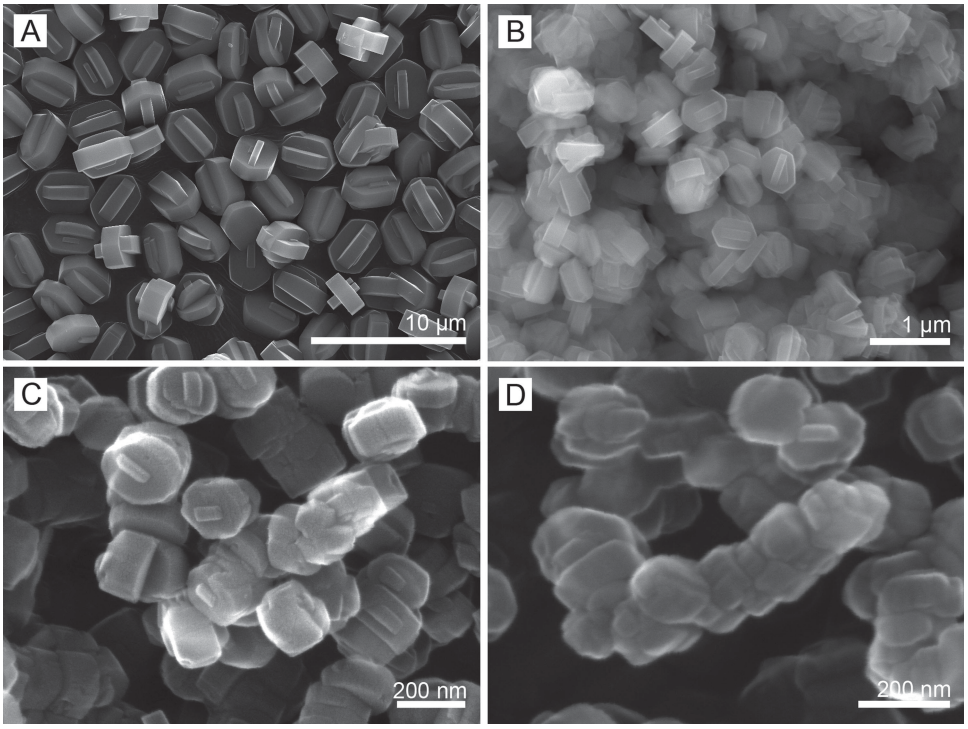

Figure 3. SEM micrographs of ZSM-5 crystals synthesized in F^- medium: (A) in the absence of seeds and in the presence of (B) 2.5 wt%, (C) 5 wt% and (D) 10 wt% seeds.

isometric and twining was less developed. The synthesis using 10 wt% seeds showed no dramatic changes in morphology and size of the crystalline product (Figure 3D). The crystallites were slightly smaller (ca. 150 nm) with morphological features very similar to the product synthesized with 5 wt% seeds.

2.1.3. Synthesis in Fluoride Medium: Effect of Temperature

The initial gel containing 5 wt% seeds yielded relatively small ZSM-5 crystals for short synthesis times. This system was used to study the effect of crystallization temperature on the crystal growth rate and crystal size. Additional experiments were performed at 443 K (Figure SI4) and 403 K (Figure SI5) and the results were compared to the results obtained at 423 K. As expected, the crystallization rate increased with temperature, whereas much longer time was needed to obtain highly crystalline product at 403 K (**Figure 4**). At 443 K, crystallization was completed after 1.5 h. Usually, an increase in crystallization temperature leads to larger zeolite crystals. However, the size of the crystals synthesized at 443 K (**Figure 5**A) did not differ from those synthesized at 423 K (Figure 2C). This result suggests that the crystallization process in the system is governed by the seeds, i.e., the amount of seeds control the ultimate crystal size. Again, coffin-like crystals with size of about 200 nm were synthesized. The result at lower crystallization temperature (403 K) was fairly different. The induction period was long; the crystallization started after 40 h and was completed within 72 h (Figure 4). The morphology of the resulting crystals was also substantially different. Instead of the well-shaped crystals synthesized at 423 K and 443 K, aggregates built of smaller crystallites were observed (Figure 5B). Their size ranged between 250 and 400 nm. These differences in size and morphology can be related to the zeolite crystallization mechanism, which is strongly influenced by the crystallization temperature. At 443 and 423 K, the degree crystallinity increased shortly after the onset of hydrothermal treatment, which increase was more pronounced for the sample prepared at 443 K. In contrast, a long induction period was observed at 403 K, suggesting reorganization in the system similar to seed-free systems. New viable nuclei are formed and continue to grow alongside the seeds. The formation of aggregates with complex morphology built up of much smaller crystals strongly supports this conclusion.

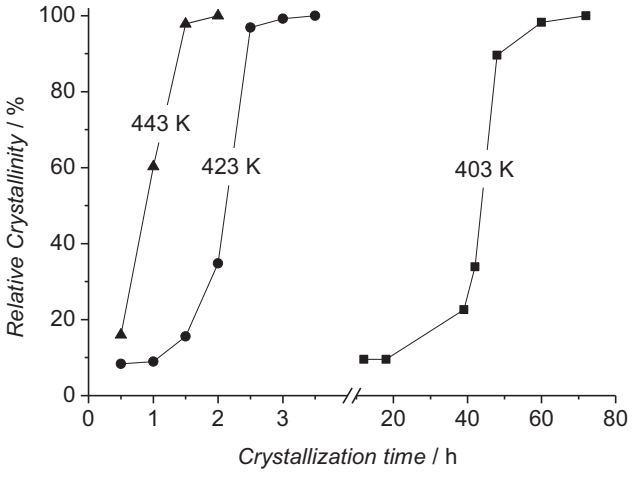

Figure 4. Crystal growth curves of ZSM-5 synthesized at different temperatures from gels containing 5 wt% seeds.

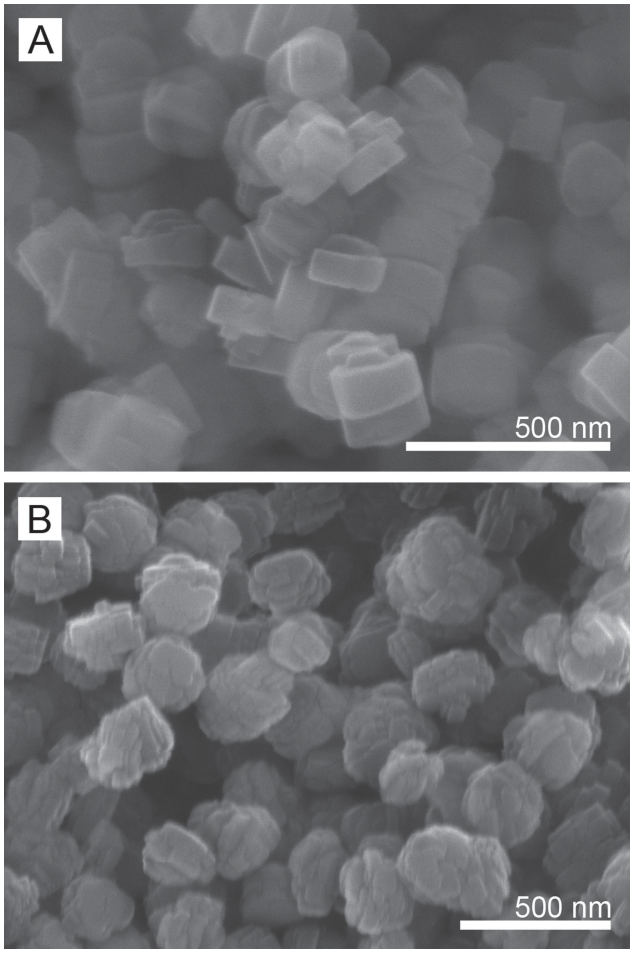

Figure 5. SEM micrographs of ZSM-5 crystals synthesized in fluoride medium with 5 wt% seeds at (A) 443 K and (B) 403 K.

2.1.4. Synthesis of Nano-ZSM-5 in OH^- Medium

Highly crystalline ZSM-5 was synthesized in OH^- medium (Figure SI6). No other crystalline phases or amorphous material were present according to XRD analysis. SEM inspection revealed that the sample consisted of complex aggregates of different sizes and random morphologies (Figure SI7A). High magnification micrographs showed that the aggregates were built of nanocrystallites with a size of ca. 50 nm (Figure SI7B). The morphology of this sample was compared to the ZSM-5 zeolite synthesized in fluoride medium at 403 K for 65 h from a gel containg 5 wt% seeds (Figure 5B). Both syntheses produced nanosized crystals. According to SEM inspection (Figure 5B and Figure SI7B), the crystals synthesized in highly alkaline medium were about three times smaller than their counterparts synthesized in fluoride medium.

2.2. Comparative Study of the Physicochemical Properties of Nano ZSM-5 Crystals Synthesized in F^- and OH^- Media

The chemical analysis of the two samples showed similar Si/Al ratio, 23.6 and 24.4 for fluoride (ZSM-5-F) and hydroxyl (ZSM-5-OH) syntheses, respectively. These values correspond to four TPA cations per unit cell, which gives Si/Al ~ 24. This is consistent with the synthesis conditions employed, namely in the absence of alkali metal cations.

The nitrogen adsorption/desorption isotherms of the two samples were very similar (**Figure 6**A). Both indicate the presence of micropores (steep increase in the gas adsorbed at low relative pressures) and mesopores (hysteresis loops in the isotherms). This is not surprising considering the similar crystallinities and morphologies of the two samples. There were differences in the mesopore size distribution as seen by the shape of the isotherms and the BJH pore size distributions (Figure 6B). The ZSM-5-F sample showed sharper peak in the range 2.5–15 nm, which may be due to the narrower crystal size distribution of this sample (Figure 5B). Nevertheless, the BET and external surface areas as well as the micro- and mesopore volumes (**Table 1**) were similar for the two samples.

Since the ultimate goal of the study was the evaluation of the catalytic properties of ZSM-5 synthesized in OH^- and F^- medium, the number of Bronsted and Lewis sites and different silanols in the two samples was of particular importance. Hence, ^1H MAS NMR experiments were performed on

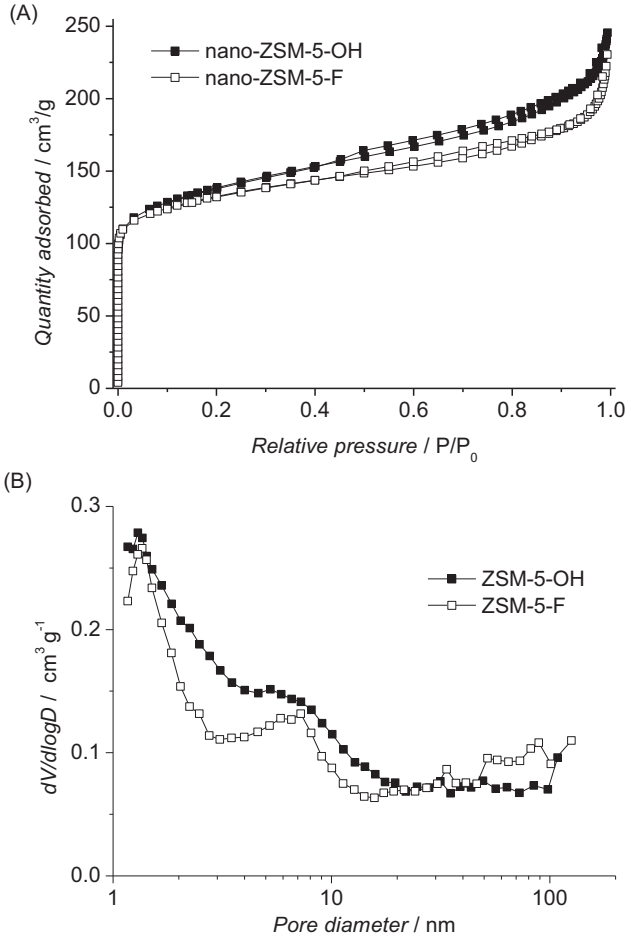

Figure 6. Nitrogen adsorption/desorption isotherms of nano ZSM-5 synthesized in OH^- and F^- media (A); BJH pore size distributions (adsorption branches) for the two samples (B).

Table 1. Specific surface area and porosity characteristics of nano ZSM-5 crystals synthesized in OH^- and F^- media.

Samples	S_{BET} [$m^2\ g^{-1}$]	V_{micro} [$cm^3\ g^{-1}$]	S_{ext} [$m^2\ g^{-1}$]	V_{meso} [$cm^3\ g^{-1}$]
ZSM-5-OH	462	0.217	69	0.15
ZSM-5-F	438	0.206	53	0.13

Table 2. ^{1}H MAS NMR shifts, assignments and intensity of OH groups in dehydrated ZSM-5-OH and ZSM-5-F samples.

Sample	$SiOH_{ext.}$		$SiOH_{def.}$	
	[d/ppm]	[µmol/g]	[d/ppm]	[µmol/g]
ZSM-5-OH	1.7	1700	2.3	2364
ZSM-5-F	1.7	678	2.3	1818

samples dehydrated at 723 K using a home-made device.[19] The obtained spectra are shown in **Figure 7** along with the Gaussian decomposition results. Four main resonances were observed for each sample. The peak at 1.7 ppm is attributed to external silanol groups, while the one at 2.3 ppm can be attributed to silanol groups in defect sites. The peak around 2.6 ppm is typical of H linked to extra-framework aluminum. Finally, the one at about 3.8 ppm corresponds to Bronsted acidic sites. In order to quantify the concentration of different proton sites, signal intensity calibration was performed using adamantane. All data are reported in **Table 2**. In agreement with previous studies, a lower amount of silanol nests was determined for the sample prepared in fluoride medium.[20] There is also a substantial difference in the surface silanols between ZSM-5-F and ZSM-5-OH samples. The smaller crystals synthesized in hydroxyl medium possess a much larger (factor of three) number of surface silanols. Protons connected to extra-framework aluminum species were found in both samples, but the associated peak was more intense in the ZSM-5-F sample.

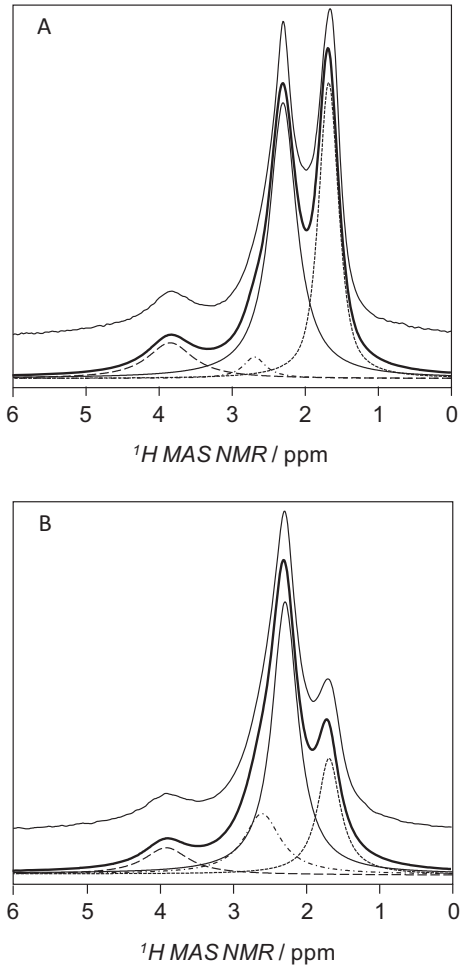

Figure 7. ^{1}H MAS NMR spectra of (A) ZSM-5-OH and (B) ZSM-5-F with decomposition of the different peaks.

^{27}Al MAS NMR spectra of ZSM-5 prepared in OH^- and F^- media are presented in Figure SI8A. Both spectra show the presence of two resonances. The first one at 55 ppm is attributed to tetrahedrally coordinated framework Al. The second at 0 ppm corresponds to hexacoordinated extra-framework Al. The two signals at 55 ppm are similar in intensity, suggesting that the two samples contain similar amount of framework Al. Figure SI8B shows the ^{29}Si MAS NMR spectra of the samples synthesized in hydroxyl and fluoride medium. In both cases, a main peak is observed at –112.8 ppm with a shoulder at –116.0 ppm. Both peaks correspond to tetrahedral Si-O-Si (Si-O-Al) environment. An additional peak is observed at 105.7 ppm, assigned to tetrahedral Si(1Al) framework. From the intensity of these resonances, a Si/Al ratio of 27 is calculated for both samples.[21] This value is slightly higher but still consistent with the chemical analysis and confirms that the Al content in the two zeolites is similar.

The NMR analysis was complemented by an IR study, **Figure 8**. Two major bands are observed in the OH-stretch vibrations region. The first one at 3610 cm^{-1} corresponds to Bronsted acid sites and the second one located at 3745 cm^{-1} is attributed to internal and surface silanols. The latter can be decomposed into three main bands at 3745 cm^{-1}, 3735 cm^{-1}, 3726 cm^{-1}, and a small broad band at 3700 cm^{-1}. According to the literature, the band at 3745 cm^{-1} is assigned to external silanol sites while the one at 3726 cm^{-1} corresponds to silanols located in micropores.[8b] In addition, a smaller band appears at 3666 cm^{-1}, usually attributed to Lewis acid sites that could be extra-framework aluminum connected to the zeolite structure.[22] It should be noted that the band at 3500 cm^{-1}, generally assigned to silanol nests, is not clearly observed due to the activation conditions (823K). In agreement with the ^{1}H MAS NMR study, the silanol contents of ZSM-5 zeolites prepared in OH^- and F^- media differ. As seen from Figure 8B, the band at 3745 cm^{-1}, with the shoulder at 3726 cm^{-1}, is more intense in the hydroxyl medium-synthesized sample. This means that ZSM-5-OH displays not only more external silanols due to the smaller crystallites, but also more internal silanols. To estimate the amounts of Brønsted and Lewis sites in the two samples, pyridine temperature-programmed desorption analysis was performed. Figure SI9 shows the infrared spectra of the two samples after pyridine adsorption. Similar Bronsted acidity, i.e.

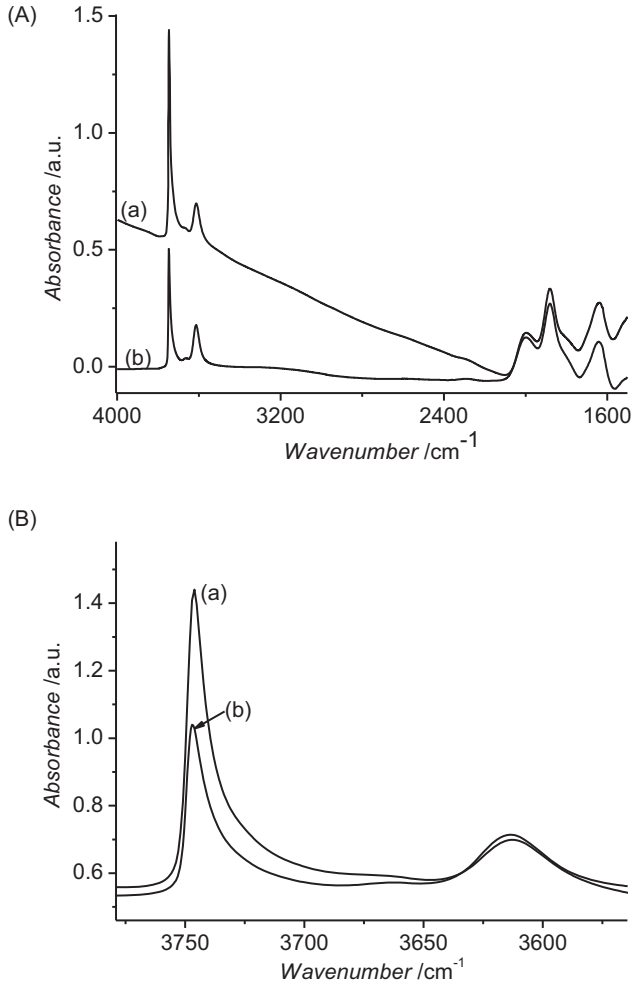

Figure 8. Infrared spectra of activated (a) ZSM-5-OH and (b) ZSM-5-F in the region 4000 –1500 cm^{-1} (A); Infrared spectra of (a) ZSM-5-OH and (b) ZSM-5-F in the OH stretching region (B).

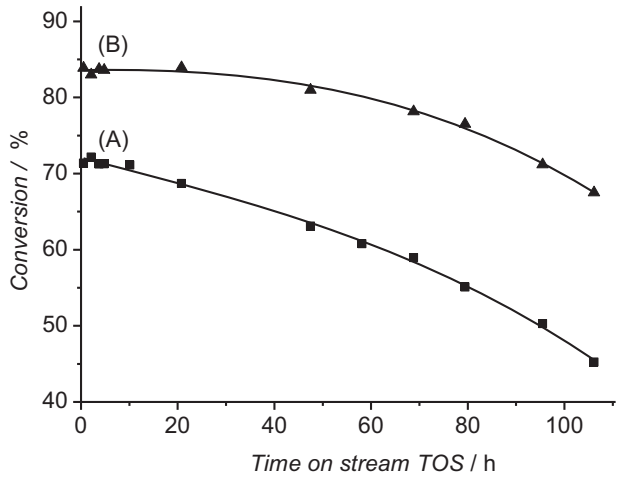

Figure 9. Conversion of methanol into hydrocarbons versus time on stream at 623 K and WHSV = 20.57 kg s mol^{-1} of (A) ZSM-5-OH and (B) ZSM-5-F.

0.242 mmol g^{-1} (ZSM-5-OH) and 0.236 mmol g^{-1} (ZSM-5-F), was measured for the two samples, but their Lewis acidity differed: 0.275 mmol g^{-1} (ZSM-5-F) and 0.213 mmol g^{-1} (ZSM-5-OH), attributed to the higher content of extra-framework Al species in ZSM-5-F. This is also in agreement with the ^{1}H MAS NMR results.

2.3. Catalytic Tests

Because of its industrial relevance and high academic interest, methanol conversion (to hydrocarbons and water) is a test reaction we selected to compare the catalytic performance of zeolites synthesized in hydroxyl and fluoride medium. **Figure 9** presents the conversion of methanol versus time on stream for the two ZSM-5 catalysts. The initial activity of ZSM-5-F (80%) was higher than that of the ZSM-5-OH (70%) despite the similar pore structures and Bronsted acidities of the two samples. The presence of larger aggregates in ZSM-5-OH and the associated diffusion limitations may be one of the reasons for the observed effect. Besides, the higher amount of Lewis acid sites in ZSM-5-F may contribute to the higher methanol conversion rate observed.

The deactivation rate of the two samples is also substantially different. Although ZSM-5-F has higher acidity in comparison to ZSM-5-OH, the deactivation is faster for ZSM-5-OH, reaching 45% conversion after 106 h (ca. 36% activity loss), while it is about 67% (ca. 16% activity loss) for ZSM-5-F. It should be mentioned that several authors have reported the more rapid catalyst deactivation for catalysts with a higher acid site density.[22] On the other hand, it is often suggested that non-framework aluminum favors coke formation. In our case, the amount of Lewis acid sites of ZSM-5-F is higher than that of ZSM-5-OH, but there is no indication that the higher Lewis acidity accelerates coke formation in the case of ZSM-5-F. Considering the presence of higher amount of silanol defects in ZSM-5-OH as shown by IR and ^{1}H MAS NMR studies, the more structural defects in this zeolite can be considered as the major contributor to faster catalyst deactivation. Structural defects in zeolites have a direct impact on their catalytic activity and deactivation. A direct correlation between coke formation and silanol defects, during xylene isomerization, has already been demonstrated by operando 2D IR spectroscopy.[23] A recent study showed that the deactivation rate of ZSM-5 during methanol conversion is strongly related to the intensity ratio of the external and internal silanol infrared bands.[8b] In particular, the presence of internal defect sites played a crucial role in the catalyst deactivation. Possibly, these internal defects are spaciously enough to accommodate the bulky penta- or hexamethylbenzene species. As a result, their residence inside these crossing would fill completely the channel or channel intersection and hinder other molecules from entering or passing through the blocked zeolite domains. These bulky hydrocarbon species evolve into coke in the course of the reaction, resulting in blockage of the access to active sites in the coked channels. Moreover, the presence of more silanols inside ZSM-5-OH makes it more hydrophilic than ZSM-5-F. In the MTH conversion on MFI, where H_2O is a major product, the more hydrophobic ZSM-5-F shifts the reaction towards the products.

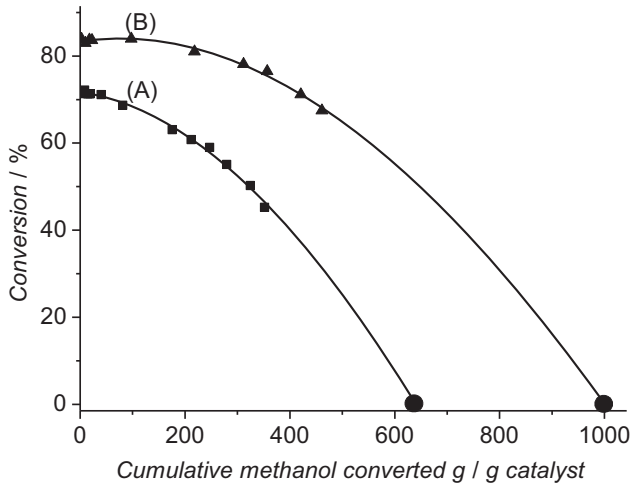

Figure 10. Methanol conversion versus the cumulative amount of methanol converted during the reaction for (A) ZSM-5-OH and (B) ZSM-5-F. Extrapolation to zero gives the total conversion capacity of the catalysts; extrapolated points are represented in black circles.

The total conversion capacity was estimated according to the method used by Bjorgen et al.[24] and plotted in **Figure 10**. The total (extrapolated) conversion capacity of ZSM-5-OH is about 641 g methanol/g of catalyst while that of ZSM-5-F is 1000 g methanol/g catalyst. These catalytic results clearly show a better overall performance of the catalysts synthesized in fluoride medium, i.e. higher initial activity and lower deactivation rate without substantial changes in the product selectivity.

3. Conclusions

ZSM-5 was synthesized in fluoride medium using nanosized silicalite-1 seeds. The crystal growth kinetics as a function of the seed content was studied for seed contents in the range 0–10 wt%. The effect of crystallization temperature on zeolite formation was also studied at 403, 423 and 443 K using 5wt% of seeds, to optimize the ZSM-5 formation in fluoride medium. The crystallization time was reduced to 1.5 h at 443 K and 3.5 h at 423 K, respectively. Highly crystalline products with sizes below 200 nm were obtained. The physicochemical and catalytic properties of ZSM-5 samples with similar Si/Al ratio synthesized in fluoride and hydroxyl medium were compared. The two materials exhibited a similar number of Bronsted acid sites, but ZSM-5-OH displayed a substantially larger number of defect sites, resulting in lower catalytic activity and faster deactivation for this sample.

The results reported demonstrate that seeded synthesis in fluoride medium can be used to decrease the zeolite crystal size, while keeping the low concentration of structural defects typical of fluoride-mediated syntheses. Thus, seed-assisted synthesis of nanozeolites in fluoride media combines the most attractive for catalytic applications features of zeolites synthesized in hydroxyl and neutral media.

4. Experimental Section

Synthesis of ZSM-5 Samples in F^- and OH^- Media: The following chemicals were used in the synthesis of ZSM-5 samples: aluminum metal powder (99.5%, Alfa Aesar), tetra-n-propylammonium hydroxide (TPAOH, 20 wt.% water solution, Alfa Aesar), fumed silica (99.8%, Aldrich), NH_4F (98%, Aldrich), tetraethyl orthosilicate (TEOS, 98%, Aldrich), aluminum isopropoxide (98%, Aldrich), tetrapropylammonium bromide (TPABr, 98%, Aldrich) and hydrochloric acid (HCl, 37%, Carlo Erba Reagents). The synthesis of ZSM-5 samples in fluoride medium (F-ZSM-5) was performed from a gel with the composition: $0.142TPABr : 0.135TPAOH : 0.072Al_2O_3 : 1.0SiO_2 : 0.616NH_4F : 20H_2O$. After mixing the initial reactants, a suspension comprising 0–10 wt% silicalite-1 seeds with respect to the silica content in the gel was added to the mixture. Seed crystals ware prepared according to a published procedure,[25] while the composition of the initial gels used in fluoride media was based on the work of Guth and co-workers.[10] The pH of the gel was then adjusted to 8.5 using HCl (0.1 M). As known from the literature,[5,6] the fluoride anions are active and act as mineralizing agent in the pH range 6–9. Consequently, we have chosen a gel with a pH which is in this range. The use of synthesis solution with higher pH (ca. 8.5) allowed accomplishing the crystallization in shorter time. The high density of the gel did not allow the use of a pH meter, thus highly accurate pH paper (Merck KGaA) was used for the pH adjustments. The resultant slurry was vigorously stirred for 1 h. The synthesis was performed at 403, 423 ,and 443 K for different periods of time to study the zeolite crystal growth kinetics. The solid product was collected by filtration, washed thoroughly with distilled water and dried at room temperature overnight. The synthesis of ZSM-5 sample in OH^- medium (OH-ZSM-5) was performed from a gel with the following composition: $0.147TPAOH : 0.0067[(CH_3)_2CHO]_3Al : 0.2TEOS : 3.507H_2O$. Aluminium isopropoxide $[(CH_3)_2CHO)_3Al]$ was firstly dissolved in TPAOH to obtain clear solution. Then TEOS was added and the resultant mixture was kept at room temperature for 6 h to hydrolyze TEOS. The ethanol formed from the hydrolysis of TEOS was evaporated using a rotary evaporator at 353 K. Then the synthesis was performed at 443 K for 120 h. The solid formed was collected by filtration, washed thoroughly and dried at room temperature overnight.

Physicochemical Characterization: Powder X-ray diffraction (XRD) patterns were obtained with a PANalytical X'Pert Pro diffractometer using Cu Kα radiation (λ = 1.5418 Å, 45 kV, 40 mA). All analyses were performed using ca. 20 mg powder loaded on a silicon wafer. The samples were studied in the 5–50° 2θ range with a scanning step of 0.0167° s^{-1}. The relative crystallinity was calculated by comparing the diffraction intensities of the five major peaks at 2θ = 23.1, 23.2, 23.6, 23.9, and 24.3° to the intensity of the most crystalline sample. Scanning electron micrographs were taken on a MIRA-LMH (TESCAN) scanning electron microscope (SEM) equipped with a field emission gun. Nitrogen adsorption measurements were performed with a Micromeritics ASAP 2020 surface area analyzer. Prior to analysis, the samples were outgassed 573 K for 12 h. Specific surface areas were determined from the BET equation. The total volume was calculated from the volume adsorbed at P/P_0 = 0.99. The t-plot method was used to calculate micropore volumes and external surface areas. IR spectra were recorded with a Nicolet Magna 550-FT-IR spectrometer at 2 cm^{-1} optical resolution. Prior to IR measurements, the catalysts were pressed into self-supporting discs (diameter: 1.6 cm, 18 mg) and were pretreated in the IR cell attached to a vacuum line at 823 K (2 K/min) for 5 h down to 10^{-6} Torr. The adsorption of pyridine was performed at 373 K. After establishing a pressure of 1 Torr at equilibrium, the cell was evacuated at 523 K in order to remove the physisorbed species. All spectra were normalized to 20 mg wafers. The amount of pyridine adsorbed on Brønsted and Lewis sites was determined using the integrated area of the bands observed at 1545 cm^{-1} and 1454 cm^{-1}, respectively. The extinction coefficients used in this study were the following: $\varepsilon(B)_{1545}$ = 1.02 and $\varepsilon(L)_{1454}$ = 0.89 cm/mol.[26] Solid-state magic angle spinning nuclear magnetic resonance spectroscopy (MAS-NMR) was used to characterize the local ^{29}Si, ^{27}Al, ^{19}F and ^{1}H environments in MFI prepared in OH^- and F^- media. All data

were recorded on a Bruker Avance 400 MHZ spectrometer using 4 mm rotor. The ^{29}Si MAS NMR spectra were recorded at 79.4 MHz, a pulse length of 4 µs (30° flip angle), a spinning rate of 14 kHz and a repetition time of 20 s. The ^{27}Al MAS NMR spectra were recorded at 104.3 MHz with a π/12 pulse length of 2.2 µs, a spinning rate of 14 kHz and a recycle delay of 1 s. ^{19}F was measured at 376.28 MHz, using Hartman-Hann echo with a π/2 pulse of 7 µs, a spinning rate of 14 kHz and a recycle delay of 5 s. Finally, ^{1}H MAS NMR was performed on samples dehydrated at 723 K for 4 h under vacuum. A Hartman-Hann echo was used with a π/2 pulse of 3.5 µs, a spinning rate of 14 kHz and a recycle delay of 2 s. TMS was used as reference for chemical shifts of ^{1}H and ^{29}Si, $Al(NO_3)_3$ (1 M) for ^{27}Al and $CFCl_3$ for ^{19}F. Elemental analysis was performed by inductively coupled plasma–atomic emission spectroscopy (ICP-AES) using an OPTIMA 4300 DV (Perkin–Elmer) instrument.

Catalytic Tests: MTH reaction tests were performed at 623 K in a fixed bed quartz reactor using 20 mg of catalyst. The reaction temperature was controlled via a thermocouple inserted in the reactor. Prior to reaction, catalysts were activated at 723 K for 4 hours at a heating rate of 1.6 K/min under air flow (50 mL min^{-1}). Then a nitrogen flow, 20 mL min^{-1}, saturated with methanol (99.6%) via a bubble saturator was introduced in the reactor. The saturator temperature (283 K) was controlled by a constant temperature bath. The methanol feed rate was estimated to 7.2% from the gas flow rate and the saturated vapour pressure (WHSV = 20.57 kg s mol^{-1}). The reactor effluents were analysed by an online gas chromatograph (GC Varian 3900; Column WCOT fused silica CP wax 52 CB 0.32 µm). To avoid condensation, the connecting lines between reactor, saturator and GC were heated to 343 K. It is noteworthy that dimethyl ether was considered as reactant and added to methanol amount in the calculation of conversion and selectivity.

Acknowledgements

The authors acknowledge the French National Scientific foundation (Agence Nationale de la Recherche – ANR) for the financial support of this work (ANR 2010 BLAN 723 1). Dr. Lakiss acknowledges the Lower Normandy Region for her research grant. The final sentence of the Conclusions section was corrected on August 23, 2013.

Received: May 6, 2013
Revised: June 3, 2013
Published online: August 9, 2013

[1] D. Breck, *Zeolite Molecular Sieves*, John Wiley & Sons, New York, USA **1974**.
[2] a) W. Vermeiren, J.-P. Gilson, *Top. Catal.* **2009**, *52*, 1131; b) A. Corma, *Chem. Rev.* **1995**, *95*, 559.
[3] V. Valtchev, G. Majano, S. Mintova, J. Perez-Ramirez, *Chem. Soc. Rev.* **2013**, *42*, 263.
[4] a) C. S. Cundy, P. A. Cox, *Microporous Mesoporous Mater.* **2005**, *82*, 1; b) V. Valtchev, L. Tosheva, *Chem. Rev.* **2013**, DOI: 10.1021/cr300439k.
[5] a) R. M. Barrer, *Hydrothermal Chemistry of Zeolites*, Academic Press, London, UK **1982**; b) C. S. Cundy, P. A. Cox, *Chem. Rev.* **2003**, *103*, 663; c) E. M. Flanigen, R. L. Patton, US Patent 4073865, **1978**; d) J.-L. Guth, H. Kessler, J. M. Higel, J. M. Lamblin, J. Patarin, A. Seive, J. M. Chezeau, R. Wey, *ACS Symp. Ser.* **1989**, *398*, 176.
[6] V. Valtchev, S. Mintova, in *Encyclopedia of Inorganic Chemistry* (Eds: C. M. Lukehart, R. A. Scott), John Wiley & Sons, Chichester **2008**, Ch. ia380, p.543.
[7] J. M. Chezeau, L. Delmotte, J. L. Guth, Z. Gabelica, *Zeolites* **1991**, *11*, 598.
[8] F. Thibault-Starzyk, A. Vimont, J.-P. Gilson, *Catal. Today* **2001**, *70*, 227; b) K. Barbera, F. Bonino, S. Bordiga, T. V. W. Janssens, P. Beato, *J. Catal.* **2011**, *280*, 196.
[9] F. L. Bleken, S. Chavan, U. Olsbye, M. Boltz, F. Ocampo, B. Louis, *Appl. Catal. A* **2012**, *447–448*, 178.
[10] J. L. Guth, H. Kessler, R. Wey, in *Stud. Surf. Sci. Catal.* (Eds: A. I. Y. Murakami, J. W. Ward) Elsevier, Amsterdam **1986**, *28*, 121.
[11] a) F. C. Meunier, D. Verboekend, J.-P. Gilson, J. C. Groen, J. Pérez-Ramírez, *Microporous Mesoporous Mater.* **2012**, *148*, 115; b) S. Ivanova, C. Lebrun, E. Vanhaecke, C. Pham-Huu, B. Louis, *J. Catal.* **2009**, *265*, 1; c) J. Arichi, B. Louis, *Cryst. Growth Des.* **2008**, *8*, 3999.
[12] L. Burel, A. Tuel, *Microporous Mesoporous Mater.* **2013**, *174*, 90.
[13] a) K. Itabashi, Y. Kamimura, K. Iyoki, A. Shimojima, T. Okubo, *J. Am. Chem. Soc.* **2012**, *134*, 11542; b) Y. Kamimura, K. Iyoki, S.P. Elangovan, K. Itabashi, A. Shimojima, T. Okubo, *Microporous Mesoporous Mater.* **2012**, *163*, 282; c) Y. Kamimura, K. Itabashi, T. Okubo, *Microporous Mesoporous Mater.* **2012**, *147*, 149; d) G. Majano, A. Darwiche, S. Mintova, V. Valtchev, *Ind. Eng. Chem. Res.* **2009**, *48*, 7084.
[14] U. Olsbye, S. Svelle, M. Bjorgen, P. Beato, T. V. W. Janssens, F. Joensen, S. Bordiga, K. P. Lillerud, *Angew. Chem.* **2012**, *124*, 5910; *Angew. Chem. Int. Ed.* **2012**, *51*, 5810.
[15] C. Fyfe, D. H. Brouwer, A. R. Lewis, J.-M. Chezeau, *J. Am. Chem. Soc.* **2001**, *123*, 6882.
[16] E. Aubert, F. Porcher, M. Souhassou, V. Petricek, C. Lacomte, *J. Phys. Chem. B* **2002**, *106*, 1110.
[17] S. K. Sur, R.G. Bryant, *Zeolites* **1996**, *16*, 118.
[18] H. M. Kao, Y.-C. Chen, *J. Phys. Chem. B* **2003**, *107*, 3367.
[19] M. Gaillard, V. Montouillout, F. Maugé, C. Fernandez, in *Stud. Surf. Sci. Catal.* (Eds: M. C. E. van Steen, L.H. Callanan), Elsevier, Amsterdam **2004**, *154*, 1679.
[20] H. Jon, Y. Oumi, K. Itabashi, T. Sano, *J. Cryst. Growth* **2007**, *307*, 177.
[21] G. Engelhardt, D. Michel, *High-Resolution Solid State NMR of Silicates and Zeolites*, John Wiley & Sons, New York, USA **1987**.
[22] a) M. Stöcker, *Microporous Mesoporous Mater.* **1999**, *29*, 3; b) M. Guisnet, L. Costa, F. R. Ribeiro, *J. Mol. Catal. A: Chem.* **2009**, *305*, 69.
[23] a) F. Thibault-Starzyk, A. Vimont, Ch. Fernandez, J.-P. Gilson, *Chem. Commun.* **2000**, *12*, 1003; b) C. Fernandez, I. Stan, J.-P. Gilson, K. Thomas, A. Vicente, A. Bonilla, J. Pérez-Ramírez, *Chem. Eur. J.* **2010**, *16*, 6224.
[24] M. Bjorgen, F. Joensen, M. S. Holm, U. Olsbye, K. P. Lillerud, S. Svelle, *Appl. Catal. A* **2008**, *345*, 43.
[25] L. Tosheva, V. P. Valtchev, *Chem. Mater.* **2005**, *17*, 2494.
[26] N. Nesterenko, F. Thibault-Starzyk, V. Montouilliout, V. Yushchenko, C. Fernandez, J.-P. Gilson, F. Fajula, I. Ivanova, *Kinet. Catal.* **2006**, *47*, 40.